Absorption of oblique incidence sound by a finite micro-perforated panel absorber

Cheng Yang[a] and Li Cheng[b]
Department of Mechanical Engineering, The Hong Kong Polytechnic University, Hung Hom, Kowloon, Hong Kong, SAR People's Republic of China

Jie Pan
School of Mechanical and Chemical Engineering, The University of Western Australia, 35 Stirling Highway, Crawley, Western Australia 6009, Australia

(Received 11 September 2012; revised 15 October 2012; accepted 28 October 2012)

In this paper, a theoretical model of a micro-perforated panel (MPP) backed by a finite cavity and flush-mounted in an infinite baffle is developed and its performance in terms of sound absorption is analyzed. The model allows an oblique incidence sound impinging upon the MPP absorber. The simplified Rayleigh integral method, thin plate theory and the acoustical impedance of the MPP are used to calculate the sound energy absorbed by the MPP's surface. Results show that the absorption coefficient of the absorber is a function of angle and frequency of the incident sound, and is controlled by the coupling between the MPP and the acoustical modes in the back cavity. In particular, grazing modes can be induced in the cavity by sound with an oblique angle of incidence, which may result in peak sound absorptions at the natural frequencies of the modes. The mechanism involved is used to explain the absorption properties of the MPP absorber for a diffuse incidence of sound.
 [http://dx.doi.org/10.1121/1.4768869]

PACS number(s): 43.50.Gf, 43.55.Ev [NX] Pages: 201–209

I. INTRODUCTION

A micro-perforated panel (MPP) has shown its potential as an effective sound absorber with non-fibrous and non-abrasive surfaces, and broadband features. Since the pioneering work by Maa,[1] there has been much effort devoted to the study of the characteristics and performance of MPP absorbers. Typically, a MPP absorber consists of a MPP and a backing air cavity (or volume). The air inside the holes of the MPP vibrates like a mass and the air inside the backing cavity works like a spring. The whole system thereby accomplishes a Helmholtz absorption effect with broadband sound absorption thanks to the high acoustical resistance and the low reactance provided by holes in sub-millimeter size.

In the pursuit of more efficient MPP absorbers, additional MPPs have been inserted into the backing cavity to form double-layered[2,3] or multiple-layer[4] MPP absorbers. Studies show that the insertion of extra MPPs would decrease the acoustic reactance and increase the acoustic resistance so that absorption band is extended toward a lower frequency range. However, when more MPPs are used, the total number of control parameters determining the absorption performance increases as well. A simulated annealing algorithm is employed[5] to streamline the parameter package of the multi-layer MPP system and this proved to be an effective solution when dealing with multiple MPP parameters.

Alternatively, the performance of a MPP absorber can be improved by modifying the coupling mechanism between the MPP and its backing cavity. In Liu and Herrin's work,[6] the backing cavity is partitioned into cells with a honeycomb structure. The micro holes within the partitioned area combined with its backing cell constitute a subsystem. In each subsystem, the air is forced to move in a direction perpendicular to the MPP surface, which is believed to be the most effective Helmholtz absorption condition. Another way of altering the coupling mechanism is to transform the rectangular cavity into a trapezoidal shape.[7] In such a case, the originally decoupled modes are allowed to couple with the MPP due to the distorted acoustic modes of the irregularly shaped cavity. As a result, the performance of the sound absorption of the conventional MPP absorber with a rectangular backing cavity in some deficient frequency ranges is significantly improved.

The aforementioned works, however, mainly focus on the normal incidence. For oblique or diffuse incidence, the equivalent circuit method was further extended by Maa.[1] The MPP impedance term remains independent of the incidence angle for its locally reactive features. However, the backing-cavity impedance becomes a parameter depending on the path difference between the transmitted and the reflected waves. Under this theoretical framework, the absorption coefficient can be readily obtained. In later works, an experiment was conducted in a reverberation room to study the characteristics of a MPP absorber in a diffuse field.[8,9] Discrepancies between theoretical and experimental results were noticed and the sound absorption peaks were found shifted to higher frequencies. Moreover, additional absorption peaks were found at higher frequencies. If the MPP parameters were selected properly, these additional

[a]This work was partially carried out while a visiting student at School of Mechanical and Chemical Engineering, The University of Western Australia.
[b]Author to whom correspondence should be addressed. Electronic mail: li.cheng@polyu.edu.hk

peaks could extend the absorption band to three, four octaves, or more. In addition, interest in oblique incidence scenarios can be seen in the work by other researchers.[10–13] In Ref. 10, Maa's formula was modified by introducing a grazing incidence into the model. In Refs. 11 and 12, an analytical model of a MPP with a cavity of infinite extent (i.e., a finite depth length and infinite borders) was developed to study the transmission loss of the MPP absorber. In Ref. 13, a MPP made of a transparent material was used as the noise barrier in a diffuse field. The proposed model was validated experimentally and proved to be sufficiently accurate for engineering applications. Although many works have been dedicated to studying the characteristics of MPP absorbers in oblique and diffuse fields, the backing cavity is usually assumed to have infinite extent. When it comes to a MPP absorber with a finite cavity size, the coupling mechanism remains unclear.

The effect of sound incidence with an arbitrary angle on the absorption characteristics of a MPP absorber backed by a finite extent cavity was investigated by Yoo *et al.*[14] It was shown that the locations of the absorption peaks in the spectrum were roughly independent of the incidence angle when the backing cavity was partitioned into an infinite array of backing segment of finite size. In this configuration, the micro-perforated holes achieve local Helmholtz resonance together with the segmented backing cavity. Thus, air is forced to move perpendicularly to the panel surface. However, when the backing space is unsegmented, the main absorption peaks move progressively to higher frequencies when the incidence angle increases. Moreover, additional absorption peaks appear when the incidence angle varies. These findings were supported by their previous experimental work,[15] but a physical explanation is still lacking. While a few experimental works reported in the literature[16,17] clearly showed the phenomena, a more comprehensive investigation of the coupling mechanism between the MPP and a backing cavity of finite extent is still needed.

In this paper, a theoretical model is developed for a MPP with a backing cavity of finite extent, flush in an infinite baffle. The surface pressure of the MPP is determined by means of the patch transfer function (PTF) method,[18] which originates from the well-known Rayleigh integral. Such a treatment allows for the consideration of an oblique incidence impinging on the MPP. The coupling mechanism between the MPP and the cavity with respect to different incidence angles is investigated. The difference between the current model and the classical model with backing cavity of infinite extent is unfolded by comparing both normal and oblique incidence cases.

II. MATHEMATICAL MODELING

The system under investigation is illustrated in Fig. 1(a). It is composed of a MPP with a trapezoidal backing cavity having an inclined wall of angle γ. Assuming an incident wave p_{in} impinging on the MPP with an incidence angle of θ and an azimuthal angle of β, the acoustic pressure outside of the cavity is $p_e = 2p_{\text{in}} + p_{\text{rad}}$, where p_{rad} is the radiated pressure at the MPP surface. Together with the surface pressure

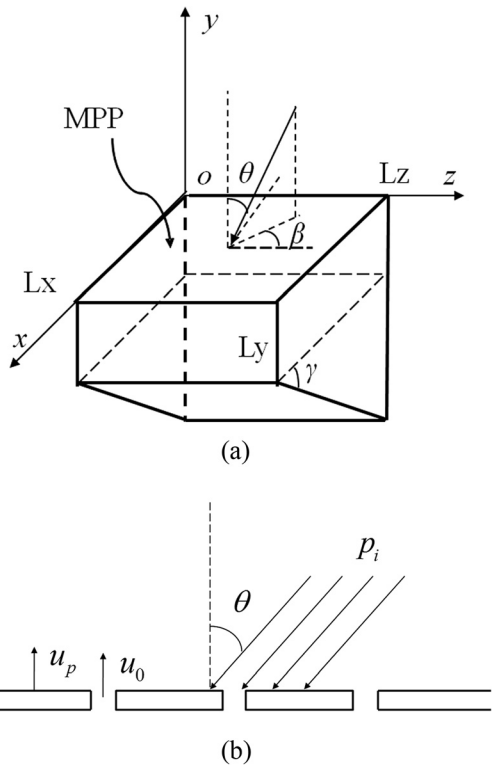

FIG. 1. Schematics of a MPP absorber excited by an oblique incidence sound in (a) 3D view and (b) 2D views of the MPP.

p_{cav} on the cavity side, the pressure difference between the two sides of the MPP generates an air mass vibration at each hole. As the diameter of the hole is much smaller than the acoustic wavelength of interest, it is appropriate to assume that the air particle velocity, u_0, is uniformly distributed within the area of each hole governed by[19]

$$Z_{\text{resist}}[u_0 - u_p] + Z_{\text{react}}u_0 = \frac{1}{\rho_0 c}[p_{\text{cav}} - (2p_{\text{in}} + p_{\text{rad}})], \tag{1}$$

where Z_{resist} and Z_{react} are the resistance and reactance of the relative specific acoustic impedances of a hole Z (divided by $\rho_0 c$), respectively, ρ_0 is the air density, c is the speed of sound in air, and u_p is the vibration velocity of the flexible MPP [Fig. 1(b)]. The air velocity is assumed to be in a direction normal to the MPP surface and pointing out of the cavity. Two versions of MPP impedance were proposed by Maa.[1,20] The difference mainly comes from the end correction term due to viscosity. As both versions basically provide the same trend in the absorption curve, the latest one for the MPP holes are used here[20]

$$\begin{aligned} Z_{\text{resist}} &= \frac{32\eta t}{\rho_0 c d^2}\left[\left(1 + \frac{K^2}{32}\right)^{1/2} + \frac{\sqrt{2}}{32}K\frac{d}{t}\right], \\ Z_{\text{react}} &= \mathrm{i}\frac{\omega t}{c}\left[1 + \left(1 + \frac{K^2}{32}\right)^{-1/2} + 0.85\frac{d}{t}\right], \end{aligned} \tag{2}$$

where $\mathrm{i} = \sqrt{-1}$, ω is the angular frequency, t is the thickness of the panel, d is the hole diameter, η is the coefficient

of viscosity, and $K = d\sqrt{\omega\rho_0/4\eta}$. For an oblique plane wave

$$p_{in} = \mathbf{P}_{\text{in}} e^{\mathrm{i}(\omega t - k_x x + k_y y + k_z z)} = \mathbf{P}_{\text{in}} e^{\mathrm{i}(\omega t - k\sin\theta\sin\beta x + k\cos\theta y + k\sin\theta\cos\beta z)}, \tag{3}$$

where k_x, k_y, and k_z are the wavenumbers in the x-, y-, and z-directions, respectively, and $\mathbf{P}_{\text{in}}$ is the incidence amplitude.

The governing equation for a flexible MPP is

$$D_p \nabla^4 w + \rho_p \frac{\partial^2 w}{\partial t^2} = p_{\text{cav}} - (2p_{\text{in}} + p_{\text{rad}}), \tag{4}$$

where D_p is the flexural rigidity of the MPP, ρ_p is the surface density, and w is the panel displacement in the y-direction. In a harmonic regime, w is expanded as

$$w = \sum_{m,n=1}^{MN} A_{mn}\varphi_{mn} e^{\mathrm{i}\omega t}, \tag{5}$$

where A_{mn} and φ_{mn} is the mnth modal amplitude and modal shape, and m and n are the modal indices in the x- and z-directions, respectively. Equation (5) is in principle valid for a MPP with any boundary condition provided the modal shape can be obtained in advance. For simplicity, assuming a simply supported boundary condition

$$\varphi_{mn} = \sin(m\pi x/L_x)\sin(n\pi z/L_z),$$

where L_x and L_z are the side lengths of the panel. The velocity is obtained with

$$u_p = \frac{\partial w}{\partial t} = \mathrm{i}\omega \sum_{m,n=1}^{MN} A_{mn}\varphi_{mn} e^{\mathrm{i}\omega t}. \tag{6}$$

For a harmonic response analysis, the time-dependence term $e^{\mathrm{i}\omega t}$ is omitted afterward. On the MPP, u_0 is a series of discrete variables at each hole. It is more convenient to describe the air motion u_0 in a spatial mean sense, as

$$\bar{u}_0 = \sigma u_0,$$

where σ is the perforation ratio in percentage. Following the standard Galerkin procedure,[21] the particle velocity over the MPP surface $\bar{u}_0$ is expanded as a series of sine functions

$$\bar{u}_0 = \sum_{m,n=1}^{MN} u_{mn}\varphi_{mn}, \tag{7}$$

where u_{mn} is the complex amplitude. With a proper truncation of the decomposition series, Eq. (7) could represent the averaged particle velocity field $\bar{u}_0$ accurately, except at the boundary edges, but this has been shown to have negligible influence on the present analysis.[7]

By substituting Eqs. (5)–(7) into Eqs. (1) and (4), multiplying both sides by φ_{mn} and applying the orthogonal property, one obtains

$$u_{mn}\bar{Z} - \mathrm{i}\omega A_{mn} Z_{\text{resist}} + \frac{4}{\rho_0 c S}\int_S (p_{\text{rad}} - p_{\text{cav}})\varphi_{mn}\, ds = -\frac{8}{\rho_0 c S}\int_S p_{\text{in}}\varphi_{mn}\, ds, \tag{8}$$

and

$$(\omega_{mn}^2 - \omega^2)A_{mn} = \frac{1}{\rho_p S}\left(\int_S 4p_{\text{cav}}\varphi_{mn}\, ds - \int_S (8p_{\text{in}} + 4p_{\text{rad}})\varphi_{mn}\, ds\right), \tag{9}$$

where $\bar{Z} = Z/\sigma$ is the overall acoustic impedance of the MPP, ω_{mn} is the mnth natural angular frequency of the panel, and S is the MPP area.

The surface pressure p_{cav} from the cavity side can be expressed in terms of acoustic modes of the rigid-walled cavity as follows:[22]

$$p_{\text{cav}} = -\frac{\mathrm{i}\rho_0 c^2 \omega}{V}\sum_{l=0}^{L}\frac{\int_S \bar{u}_a\psi_l\, ds}{\Lambda_l(\omega^2 - \mathrm{i}\xi_l\omega\omega_l - \omega_l^2)}\psi_l, \tag{10}$$

where ψ_l is the lth acoustical mode of the cavity at $y = 0$, ζ_l and Λ_l are the modal damping and the generalized acoustic mass of the lth cavity mode, respectively, V is the cavity volume, and $\bar{u}_a$ is the surrounding air particle velocity in the vicinity of the MPP, which is defined as

$$\bar{u}_a = (1 - \sigma)u_p + \bar{u}_0. \tag{11}$$

For a rigid MPP, only the air motion at the orifices contributes to $\bar{u}_a$, so the u_p term is null when calculating the surrounding air particle velocity.

For a MPP absorber inserted in an infinite baffle, the surface pressure is approximated by the PTF approach.[18] Inspired by the well-known Rayleigh integral, the panel is discretized into small patches and each small patch vibrates like a monopole source (the patch size should be smaller than half of the wavelength of interest). The radiation pressure p_{rad} at each patch is contributed by the pressure radiated by the patch itself and by the other patches. Therefore, the self-radiation and mutual radiation impedances (a detailed process for obtaining the radiation impedance can be found in the Appendix in Ref. 18) are defined as

$$Z_{pp} = \frac{p_{\text{rad}}^p}{\bar{u}_a^p} = \rho_0 c[1 - e^{-\mathrm{i}ka}],$$
$$Z_{pq} = \frac{p_{\text{rad}}^p}{\bar{u}_a^q} = \frac{1}{2\pi}\mathrm{i}\rho_0\omega\frac{e^{-\mathrm{i}kd_{pq}}}{d_{pq}}S_q, \tag{12}$$

where the superscripts p and q indicate the patch indices, k is the wave number $k = \omega/c$, d_{pq} is the center distance between patch p and q, S_q is the surface area of the patch q, and a is the radius of an equivalent circular patch S_p.

After some manipulation and by defining

$$Z_{\text{cav},mnm'n'} = -\frac{i\rho_0 c^2 \omega}{V} \sum_{l=0}^{L} \frac{\int_S \psi_l \varphi_{mn}\, ds \int_S \psi_l \varphi_{m'n'}\, ds}{\Lambda_l(\omega^2 - i\xi_l \omega\omega_l - \omega_l^2)}$$

and

$$Z_{\text{rad},mnm'n'} = \sum_{p=1}^{P}\sum_{q=1}^{P} Z_{pq}\varphi_{mn}^{q}\varphi_{m'n'}^{p},$$

where P is the total patch number on the MPP; Eqs. (8) and (9) can be expressed in a matrix form as

$$[\bar{Z}]\{u_{mn}\} - i\omega[Z_{\text{resist}}]\{A_{mn}\} + \frac{4}{\rho_0 cS}([Z_{\text{rad},mnm'n'}] - [Z_{\text{cav},mnm'n'}])\{u_{mn}\} = \{I_{mn}\}, \quad (13)$$

where

$$I_{mn} = -\frac{8}{\rho_0 cS}\int_S p_{in}\varphi_{mn}\, ds,$$

and

$$(\omega_{mn}^2 - \omega^2)\{A_{mn}\} + \frac{4}{\rho_p S}([Z_{\text{rad},mnm'n'}] - [Z_{\text{cav},mnm'n'}]) \times \Big((1-\sigma)i\omega\{A_{mn}\} + \{u_{mn}\}\Big) = \{I_{mn}\}, \quad (14)$$

where [-] is a matrix and {-} is a vector containing all the mode indices. The unknown variables u_{mn} and A_{mn} in Eqs. (13) and (14) can be solved provided that a sufficient number of modes are considered. Note that the model developed here is also applicable to an irregularly shaped cavity provided the cavity modes are known. The sound absorption coefficient of the MPP absorber can be calculated as

$$\alpha_{\theta,\beta} = \frac{\rho_0 c\int_S \text{Re}(p_e^* \cdot \bar{u}_a)\, ds}{|\text{P}_{\text{in}}|^2 S}, \quad (15)$$

where an averaged absorbed energy by the MPP absorber in a unit area is defined as

$$\Pi_{\text{averaged}} = \frac{1}{2S}\int_S \text{Re}(p_e^* \cdot \bar{u}_a)\, ds, \quad (16)$$

where the asterisk denotes the complex conjugate.

For diffused incidence,[23]

$$\bar{\alpha} = \frac{1}{2\pi}\int_0^{2\pi}\left(\int_0^{\pi/2} \alpha_{\theta,\beta}\sin 2\theta\, d\theta\right) d\beta. \quad (17)$$

III. NUMERICAL SIMULATIONS

A. Oblique incidence on a MPP absorber

A MPP absorber subject to sound of an oblique incidence is numerically studied in this section. The sound absorption coefficient ($\alpha_{\theta,\beta}$) is calculated by keeping $\beta = 90°$ for simplicity. With this treatment, excitation of the plane wave is constant along the z axis so that the influences from the modes having the mode index (*,*,n_z) ($n_z \neq 0$) are not activated. This is a particular case under the general three-dimensional (3D) framework, which is not exactly a two-dimensional (2D) filed in the most rigorous sense. Such a treatment is not a limitation of the present model but it avoids introducing too many modes that may complicate an understanding of the underlying physics. A rectangular cavity ($\gamma = 0°$) is first used in the analysis for its clearly identified mode shapes, which are helpful in investigating the underlying coupling mechanism. For the sake of convenience, the vibration of the panel is ignored in the following numerical simulations as the vibration was found to mainly contribute to the sound absorption in the vicinity of panel resonances.[19] The parameters of the cavity and the MPP are listed in Table I.

TABLE I. MPP absorber parameters.

L_x	L_y	L_z	Perforation ratio σ	Hole diameter d	Panel thickness t
0.4 m	0.15 m	0.3 m	0.5%	0.2 mm	0.2 mm

The sound absorptions of the absorber with three incidence angles 0°, 45°, and 90° are calculated using the current model and plotted in Fig. 2. It can be seen that $\alpha_{\theta,\beta} > 1$ at some frequencies. This phenomenon can be explained as follows: for a MPP absorber flush-mounted in an infinite baffle, the impedance discontinuity between the baffle and the MPP generates a so-called "edge effect."[24] This phenomenon brings increased energy from the surrounding baffle region into the border of the MPP, particularly at low frequencies. According to Eq. (15), $\alpha_{\theta,\beta}$ is defined as the ratio of the total absorbed energy by the MPP to the incident energy directly impinging on the MPP. The additional energy from the diffraction wave is not taken into account in the denominator term, leading to an overestimation of the energy absorption coefficient. A more detailed explanation of the increased sound absorption due to edge effect can be found in the previous work.[25]

In Fig. 2, the first absorption peak appears at roughly the same frequency in all three incidence cases, and is

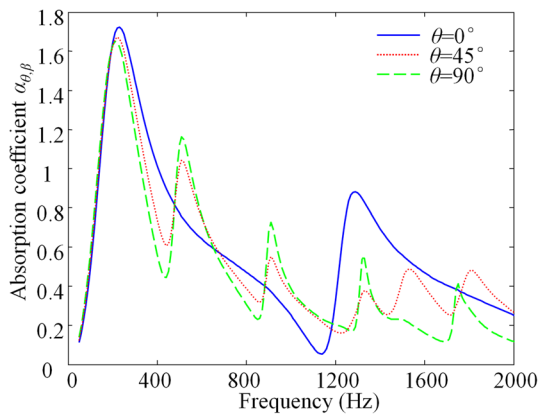

FIG. 2. (Color online) Sound absorption coefficients with respect to different incidence angles.

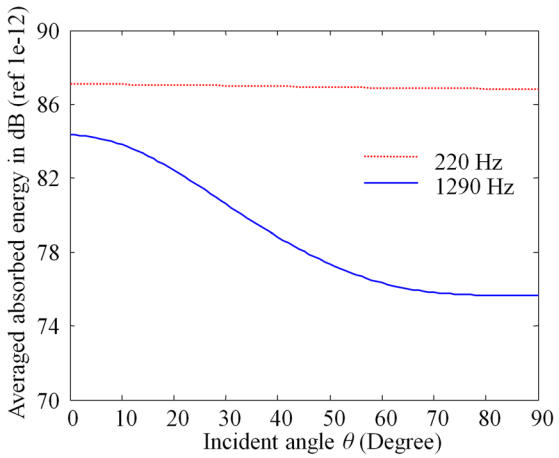

FIG. 3. (Color online) Average energy absorbed by the MPP absorber at 220 Hz and 1290 Hz.

dominated by the air stiffness of the cavity (i.e., the air volume). The average energy [Eq. (16)] absorbed by the MPP with respect to θ is examined at 220 Hz and 1290 Hz (the two absorption peaks when $\theta = 0°$) in Fig. 3. It is observed that the average absorbed energy at 220 Hz is roughly independent of θ. This indicates that if there is no change in the volume of the backing cavity, the first absorption peak maintains a constant value and occurs at a fixed frequency.

The first nine acoustic mode shapes of the cavity in x-y plane at $z = L_z/2$ are presented in Fig. 4 with the MPP locates at the top. According to the acoustical properties, the modes that are moving perpendicularly to the MPP are defined as non-grazing mode; the modes that are moving parallel to the MPP are defined as grazing mode and the modes that can move orthogonally are defined as cross mode.

At 1290 Hz, corresponding to the second peak ($\theta = 0°$), sound absorption is actually associated with the third mode of the backing cavity, i.e., non-grazing mode. It can be seen from Fig. 2 that $\alpha_{\theta,\beta}$ varies with the incidence angle for the three cases, while Fig. 3 confirms that the average sound absorption at that particular frequency is sensitive to the changes of the incidence angle in a relatively large region (roughly from 20° to 60°). Compared with the normal incident case, more ripples are found in the $\alpha_{\theta,\beta}$ spectrum with the oblique incident wave.

The appearances of dips and peaks were shown to be the consequence of the coupling between the MPP and the non-grazing modes in the normal incidence case.[7] A more detailed examination is needed to reveal the coupling mechanism between the MPP and the backing cavity in the case of oblique incidence. This is done by examining two extreme cases, i.e., $\theta = 0°$ and $\theta = 90°$. The current system is believed to have low modal density within the frequency range of interest. Each pair of peaks and dips are then dominated by one specific cavity mode. Based on this assumption, two pairs of peaks and dips at $\theta = 0°$ and 90° are examined.

Figure 5 illustrates the contribution of the first ten cavity modes (including the zeroth mode) toward the total sound pressure in the backing cavity at these selected frequencies. The modal contribution is demonstrated in terms of modal amplitude. According to Eq. (10), the modal amplitude for the lth mode is defined as

$$-\frac{i\rho_0 c^2 \omega}{V} \frac{\int_S \bar{u}_a \psi_l \, ds}{\Lambda_l(\omega^2 - i\xi_l \omega \omega_l - \omega_l^2)}. \tag{18}$$

For a normal incidence (first row), except at the zeroth mode, the 3rd mode dominates, which is classified as a non-grazing mode according to Fig. 4. Other modes have only a negligible contribution. When $\theta = 90°$, the contribution of the grazing modes is noticeable. In particular, at frequencies near the resonance of the 1st mode (the first two columns in the second row), the 1st mode is predominant. Consequently, the dominant coupling effect yields a pair of peaks and dips in Fig. 2, and the dip roughly occurs at the resonance of the 1st mode. Likewise, after further checking of the dips (850 Hz, 1270 Hz, and 1690 Hz) in the curve, these frequencies approximately match the resonance frequencies of the grazing modes 2, 5, and 7, respectively.

The aforementioned comparison reveals the different coupling mechanisms for the MPP absorber subjected to grazing incidence. First, a grazing incidence wave will activate the grazing cavity modes. These modes contribute

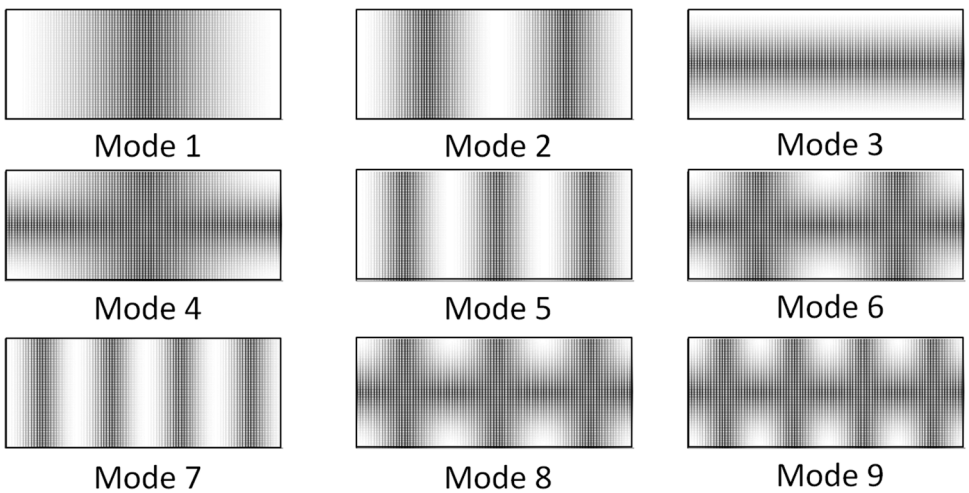

FIG. 4. The first nine acoustic modes (excluding the zero mode) of a rectangular backing cavity in the x-y plane (mode index in z axis is 0) with the MPP at the top. Modes 1, 2, 5, and 7 are denoted as grazing modes; mode 3 is denoted as a non-grazing mode; and modes 4, 6, 8, and 9 are denoted as cross modes.

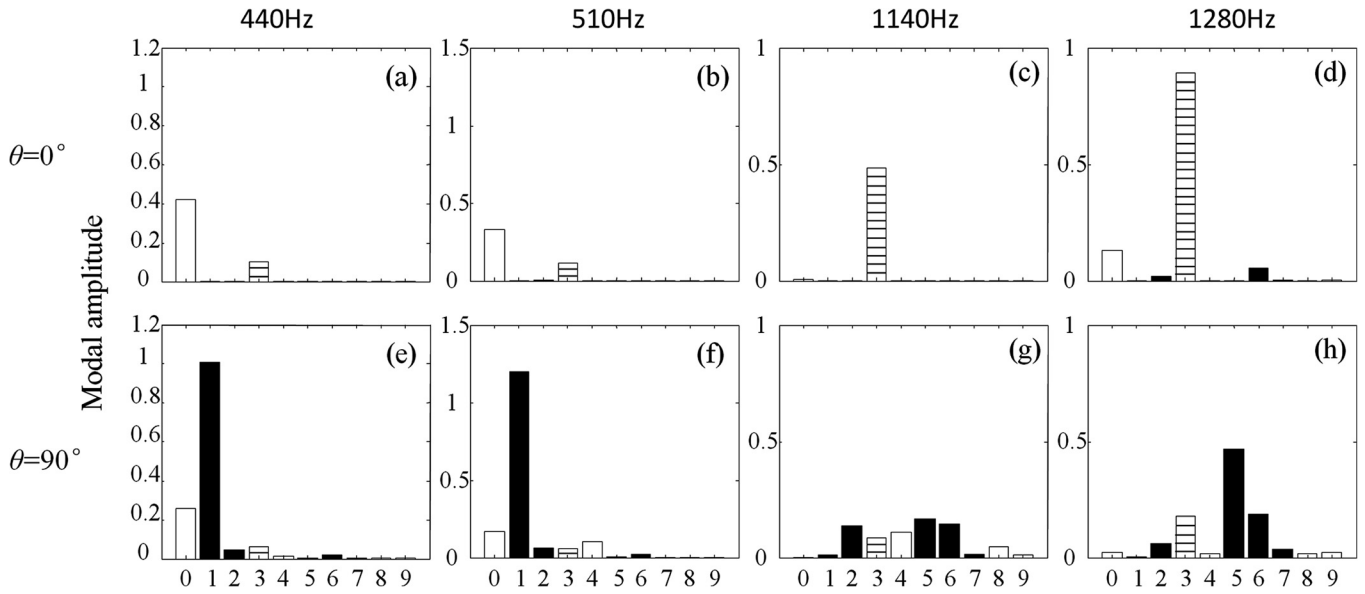

FIG. 5. Modal amplitudes of the first ten modes observed at different frequencies and incidence angles: (a) 440 Hz, $\theta = 0°$; (b) 510 Hz, $\theta = 0°$; (c) 1140 Hz, $\theta = 0°$; (d) 1280 Hz, $\theta = 0°$; (e) 440 Hz, $\theta = 90°$; (f) 510 Hz, $\theta = 90°$; (g) 1140 Hz, $\theta = 90°$; (h) 1280 Hz, $\theta = 90°$ [■: grazing modes; ▤: non-grazing modes; □: other modes (zeroth mode + cross modes)].

effectively to determining the absorption performance of the MPP absorber. Second, each grazing wave generates a pair of spectral peaks and dips, with the former corresponding to the coupled natural frequency of the MPP-cavity system, while the latter roughly occurs at the resonance of the corresponding grazing mode of the hard-walled backing cavity. Third, a grazing mode has a predominant contribution to the frequencies around its resonance frequency when subjected to a grazing incident wave.

As the absorption is dominated by different types of modes at 0° and 90°, the control mechanism must vary with the change of incidence angle. Concerning this, the variations of the modal contribution by the incidence angle are investigated at 510 Hz and 1290 Hz, which belong to absorption peaks at two extreme angles, respectively. It is noted that these two frequencies are arbitrarily selected. The coupling variation rule applies to other frequencies as well.

It can be observed in Fig. 6(a) that the contribution of the 1st mode gradually increases with the incidence angle. This indicates a strengthened coupling between the MPP and the 1st cavity mode when the incident wave varies from normal to grazing. From 0° to 90°, the initially decoupled grazing mode gradually couples to the MPP and reaches its maximum at 90°. For the other modes, only slight changes are observed during the variation of the angle. It is noted, however, that the 3rd mode continuously decreases when the angle increases. This implies that the coupling of a non-grazing mode becomes weaker as the incidence decreases to a grazing angle. A contrary behavior in the variation of the contribution shows that a grazing mode becomes more effective and a non-grazing mode becomes less effective at absorption as θ increases. Therefore, the strongest coupling is found at 90° for the grazing mode and 0° for the non-grazing mode.

The modal amplitude variation at 1290 Hz is shown in Fig. 6(b). At this frequency, the 3rd mode (a non-grazing mode) and the 5th mode (a grazing mode) dominate at 0° and 90°, respectively. A coupling variation trend similar to that at 510 Hz can be found. Moreover, the maximum couplings of the 4th and 6th modes happen at neither 0° nor 90° but in between. Recalling the mode shapes of these two modes, they are neither grazing modes nor non-grazing

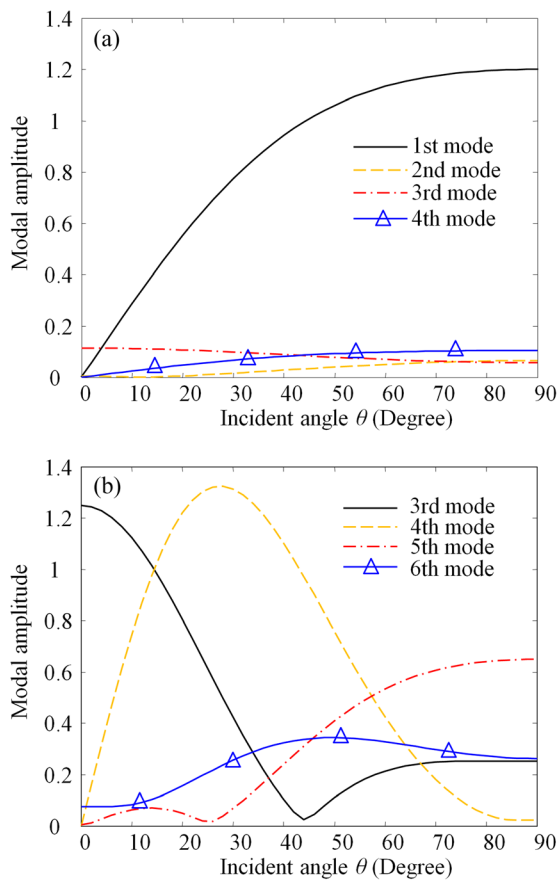

FIG. 6. (Color online) Variation of modal contribution versus incidence angle observed at different frequencies: (a) 510 Hz and (b) 1280 Hz.

modes. This kind of mode is termed as a cross mode in this paper. According to its mode characteristics, the cross mode can be effectively excited by both the normal incidence and the grazing incidence. Therefore, the strongest coupling takes place after a trade-off between the two extreme angles and may have the maximum modal contribution between 0° and 90°. Meanwhile, the cross mode also influences the coupling strength of the grazing mode and non-grazing. This is an indirect coupling process between modes.[26] Each mode is first coupled to the MPP, and then interacts with each other through the MPP. As can be seen, the 3rd and 5th modes have local extrema due to the indirect coupling effect. It can be predicted, if the cross type mode has a slight contribution to the absorption (thereby a less indirect coupling effect to the grazing and non-grazing modes), the local minimum values will not appear in the curve.

The overall profile of the sound absorption coefficient of a MPP absorber, $\alpha_{\theta,\beta}$, at different incidence angles is presented in Fig. 7. The spectral peaks at 90° gradually vanish when the incidence varies from a grazing incidence to a normal incidence. This reinforces the variation of the coupling mechanism between the MPP and the cavity. From 90° to 0°, the dominant role of the grazing mode declines and the non-grazing mode is enhanced. Therefore, only the first absorption peak (cavity volume-controlled) and the peak which is induced by the 3rd mode (a non-grazing mode) remain in the spectrum at $\theta = 0°$.

B. Diffuse field incidence on a MPP absorber

It is expected that, in the diffuse field, different angles would arouse different modes in the sound absorption. Each type of mode couples to the MPP at its effective angle and causes absorption peaks in the spectrum. Indeed, these absorption peaks are observed in the $\bar{\alpha}$ spectrum (Fig. 8). However, at a frequency where no effective coupling takes place (i.e., none of the cavity modes are effectively coupled to the MPP at any incidence angle), a big trough will be found. For example, at around 1200 Hz, the absorption performance is rather poor. This can be improved by using a trapezoidal backing cavity[7] with leaning angles of $\gamma = 30°$ or 60° as shown in Fig. 8. This points to the potential of using an irregularly shaped cavity to enhance the sound absorption performance of the MPP absorber at strategic frequency bands. The trapezoidal configuration reconstructs the rectangular cavity modes, and thus the modes that are initially decoupled to the MPP can become well coupled. As can be seen in Fig. 8, the two trapezoidal cavity configurations improve performance in the trough at around 1200 Hz. It is noted that the two trapezoidal configurations in this paper are used to illustrate the advantages of a trapezoidal cavity in abating noise from a diffuse field. No effort is made to pursue an optimal cavity configuration.

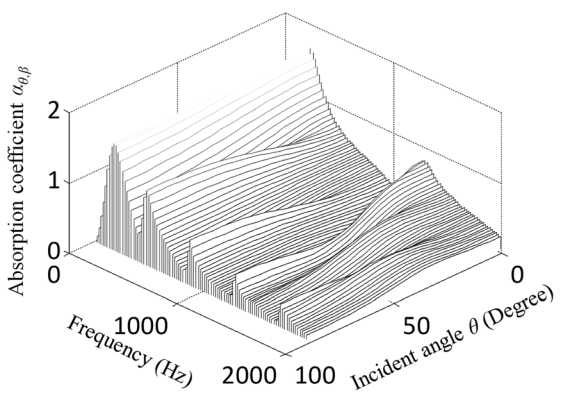

FIG. 7. Sound absorptions at different incidence angles.

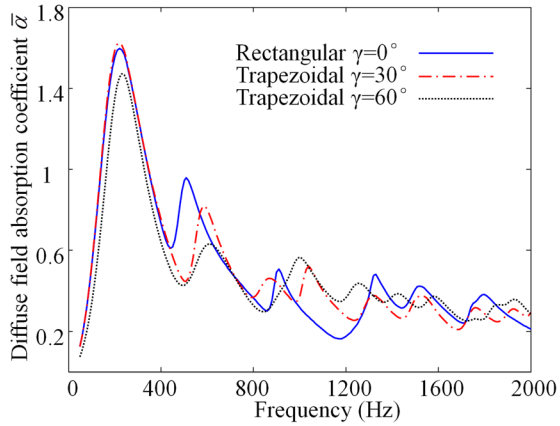

FIG. 8. (Color online) Diffuse field sound absorption coefficients for three configurations.

C. Effects of the backing cavity environment on the absorption of a MPP absorber

In this section, the oblique incidence model of a MPP absorber backed by cavity of infinite extent proposed by Maa[20] is employed as a benchmark for comparison. The absorption configuration used is the same as in the Secs. III A and III B. In order to approximate the same environment for comparison, as in the benchmark model, a special treatment is carried out on the modal damping ζ_{mn} of the cavity. In the following simulations, the modal dampings of the non-grazing modes are set at 0.5%. For the other modes, 0.5% (small), 5% (moderate), and 50% (high) are used, respectively.

Two incidence angles, $\theta = 0°$ and $\theta = 30°$, are used for comparison. As shown in Fig. 9(a), for a normal incidence, the change of modal damping will not affect $\alpha_{\theta,\beta}$. This reinforces the fact that a MPP is strongly coupled to the non-grazing modes when the absorber is subject to normal incidence. In the normal incidence case, the current model agrees with the benchmark model at most frequencies. A significant discrepancy at low frequencies is caused by the edge effect, which has been discussed in Sec. III A.

With $\theta = 30°$ [Fig. 9(b)], the value of modal damping becomes an important parameter in determining the absorption. For a small modal damping of 0.5%, multiple peaks appear in the spectrum, which are the result of strong coupling between the MPP and different types of cavity modes. At this incidence angle, both the grazing and non-grazing modes contribute effectively to the absorption. Thus, the absorption dip does not exactly coincide with the resonance of the corresponding mode but has a frequency shift. For a moderate modal damping of 5%, the coupling-induced peaks can still be found in the spectrum. However, an obvious

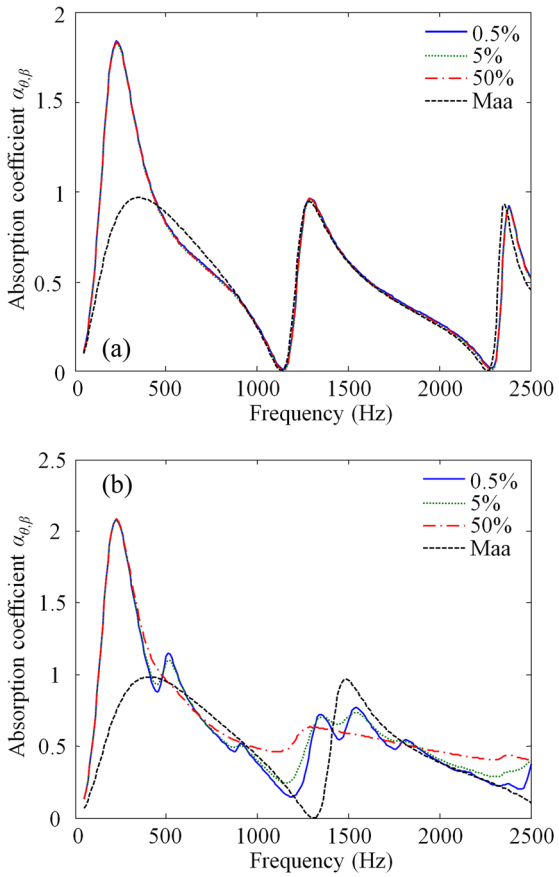

FIG. 9. (Color online) A comparison of the current model with Maa's model. The modal dampings of the non-grazing modes are set at 0.5%, with three different dampings for the other modes: (a) $\theta = 0°$ and (b) $\theta = 30°$.

damping effect is noticed. Indeed, when the modal damping increases, the damped modes become less effective at sound absorption. Therefore, the peaks and dips that are dominated by these damped modes are less noticeable. For a high modal damping of 50%, peaks that are dominated by the grazing modes disappear, and only the peaks induced by the non-grazing modes remain. The disappearance of these peaks is easy to understand, as the dominated modes are over-damped and become ineffective in the coupling. Moreover, the large modal damping will damp both the traveling wave and the reflecting wave in the x- and z-directions within the cavity. This neutralizes all grazing modes of the backing cavity.

In all, the current model has a similar trend as the benchmark model with differences in the details. It is relevant to note that different modes contribute differently to the sound absorption. Therefore, a single damping value assigned to all cavity modes may not produce exactly the same backing cavity environment as in the benchmark model. This may be a plausible reason that explains why the current model deviates from the benchmark model.

IV. CONCLUSIONS

A theoretical model of a MPP backed by a cavity of finite extent and set flush in a baffle is established in the current paper. The utilization of the simplified Rayleigh integral method allows for the consideration of oblique and diffuse incidences impinging on the MPP. Analysis shows that for a normal incidence, the non-grazing modes play an important role in determining the sound absorption performance, while for a grazing incidence, the grazing modes become dominant. The variation of the modal contribution illustrates that the initial decoupled grazing mode is gradually induced to couple with the MPP when the incidence varies from normal to near grazing, simultaneously diminishing the effects of the non-grazing mode. Consequently, in a diffuse field, multiple peaks are present in the spectrum as a result of strong coupling between one cavity mode and the MPP at its best coupling incidence angle. However, at frequencies where no effective coupling takes place over the whole incidence angle range, only poor sound absorption is found. This problem is overcome by using a trapezoidal backing cavity that allows one to tune the coupling strength to achieve the desired sound absorption.

The effect of the backing cavity environment is also studied. For a normal incidence, the current model agrees well with the benchmark model at most frequencies, except at the low frequencies, which are affected by the edge effect due to impedance discontinuity between the MPP and the rigid baffle. In addition, the absorption performance is independent of the modal damping in the x- and z-directions. At an oblique incidence, the performance is more sensitive to changes in the modal damping. This is because these modes are strongly coupled to the MPP at an oblique incidence. Therefore, absorption peaks induced by grazing modes appear if a small damping is used, and disappear if these modes are over-damped.

ACKNOWLEDGMENTS

C.Y. is grateful for the financial support from the Research Student Attachment Program at The Hong Kong Polytechnic University. The authors wish to acknowledge a grant from Research Grants Council of Hong Kong Special Administrative Region, China (Grant No. PolyU 5140/09E).

[1]D. Y. Maa, "Theory and design of microperforated-panel sound-absorbing construction," Sci. Sin. **XVIII**, 55–71 (1975).
[2]Z. M. Zhang and X. T. Gu, "The theoretical and application study on a double layer microperforated sound absorption structure," J. Sound Vib. **215**, 399–405 (1998).
[3]K. Sakagami, T. Nakamori, M. Morimoto, and M. Yairi, "Double-leaf microperforated panel space absorber: A revised theory and detailed analysis," Appl. Acoust. **70**, 703–709 (2009).
[4]D. H. Lee and Y. P. Kwon, "Estimation of the absorption performance of multiple layer perforated panel systems by transfer matrix method," J. Sound Vib. **278**, 847–860 (2004).
[5]H. Ruiz, P. Cobo, and F. Jacobsen, "Optimization of multiple-layer microperforated panels by simulated annealing," Appl. Acoust. **72**, 772–776 (2011).
[6]J. Liu and D. W. Herrin, "Enhancing micro-perforated panel attenuation by partitioning the adjoining cavity," Appl. Acoust. **71**, 120–127 (2010).
[7]C. Q. Wang, L. Cheng, J. Pan, and G. H. Yu, "Sound absorption of a micro-perforated panel backed by an irregular-shaped cavity," J. Acoust. Soc. Am. **127**, 238–246 (2010).
[8]K. Liu, C. Nocke, and D. Y. Maa, "Experimental investigation on sound absorption characteristics of microperforated panel in diffuse fields," Acta. Acust. **25**, 211–218 (2000) (in Chinese).
[9]D. Y. Maa and K. Liu, "Sound absorption characteristics of microperforated absorber for random incidence," Acta. Acust. **25**, 289–296 (2000) (in Chinese).

[10]M. Wu, "Micro-perforated sheet metal and its application to silencer design (A)," J. Acoust. Soc. Am. **93**, 2309 (1993).
[11]D. Takahashi and M. Tanaka, "Flexural vibration of perforated plates and porous elastic materials under acoustic loading," J. Acoust. Soc. Am. **112**, 1456–1464 (2002).
[12]M. Toyoda and D. Takahashi, "Sound transmission through a microperforated-panel structure with subdivided air cavities," J. Acoust. Soc. Am. **124**, 3594–3603 (2008).
[13]F. Asdrubali and G. Pispola, "Properties of transparent sound-absorbing panels for use in noise barriers," J. Acoust. Soc. Am. **121**, 214–221 (2007).
[14]T. Yoo, J. S. Bolton, J. Alexander, and D. Slama, "Absorption from finite-sized microperforated panels at arbitrary incidence angles," in *Proceedings of the 15th ICSV*, Daejeon, Korea (2008).
[15]N. R. Londhe, J. S. Bolton, T. Yoo, J. H. Alexander, and D. F. Slama, "Random incidence sound absorption coefficient of micro-perforated absorbers," in *Proceedings of NOISE-CON2007*, Reno, NV (2007).
[16]N. Hillereau, A. A. Syed, and E. J. Gutmark, "Measurements of the acoustic attenuation by single layer acoustic liners constructed with simulated porous honeycomb cores," J. Sound Vib. **286**, 21–26 (2005).
[17]G. Li and C. K. Mechefske, "A comprehensive experimental study of micro-perforated panel acoustic absorbers in MRI scanners," Magn. Reson. Mater. Phys., Biol., Med. **23**, 177–185 (2010).
[18]J. D. Chazot and J. L. Guyader, "Prediction of transmission loss of double panels with a path-mobility method," J. Acoust. Soc. Am. **121** 267–278 (2007).
[19]Y. Y. Lee, E. W. M. Lee, and C. F. Ng, "Sound absorption of a finite flexible micro-perforated panel backed by an air cavity," J. Sound Vib. **287**, 227–243 (2005).
[20]D. Y. Maa, "Potential of microperforated panel absorber," J. Acoust. Soc. Am. **104** 2861–2866 (1998).
[21]L. Meirovitch, *Fundamentals of Vibrations* (McGraw-Hill, Boston, 2001), pp. 529–533.
[22]L. Cheng, Y. Y. Li, and J. X. Gao, "Energy transmission in a mechanically-linked double-wall structure coupled to an acoustic enclosure," J. Acoust. Soc. Am. **117**, 2742–2751 (2005).
[23]F. Fahy and P. Gardonio, *Sound and Structural Vibration: Radiation, Transmission and Response*, 2nd ed. (Academic, London, 2007), pp. 1–293.
[24]P. E. Sabine, "What is measured in sound absorption measurements," J. Acoust. Soc. Am. **6**, 239–245 (1935).
[25]L. Maxit, C. Yang, L. Cheng, and J. L. Guyader, "Modeling of micro-perforated panels in a complex vibro-acoustic environment using patch transfer function approach," J. Acoust. Soc. Am. **131**, 2118–2130 (2012).
[26]K. S. Sum and J. Pan. "Effects of the inclination of a rigid wall on the free vibration characteristics of acoustic modes in a trapezoidal cavity," J. Acoust. Soc. Am. **119**, 2201–2210 (2006).